Long Title: Safety and data quality of simultaneous EEG-fMRI using multi-band fMRI imaging

Short Title: Safety and data quality of simultaneous EEG-fMRI using multi-band fMRI imaging

Author List:

Maximillian K. Egan*[1,2], Ryan Larsen*[2], Jonathan Wirsich[2,3], Brad P. Sutton[2,4], Sepideh Sadaghiani[1,2]

* These authors contributed equally

[1]Psychology Dept., Univ. of Illinois At Urbana-Champaign, Urbana, IL, [2]Beckman Institute for Advanced Science and Technology, Univ. of Illinois At Urbana-Champaign, Urbana, IL, [3] EEG and Epilepsy Unit, Univ. Hospitals and Faculty of Medicine of Geneva, Geneva, Switzerland, [4]Bioengineering Dept., Univ. of Illinois At Urbana-Champaign, Urbana, IL

Abstract

Purpose

Simultaneously recorded electroencephalography and functional magnetic resonance imaging (EEG-fMRI) is highly informative yet technically challenging. Until recently, there has been little information about the data quality and safety when used with newer multi-band (MB) fMRI sequences. Here, we assessed heating-related safety of a MB protocol on a phantom, then evaluated EEG quality recorded concurrently with the MB protocol on humans.

Materials and Methods

We compared radiofrequency (RF)-related heating and magnetic field magnitude (B_1^+RMS) of a fast MB fMRI sequence with whole-brain coverage (TR=440ms, MB factor=4) against a previously recommended, safe single-band (SB) sequence using a phantom outfitted with a 64-channel EEG cap. Temperatures were recorded at the ECG and TP7 electrodes using a fluoroptic thermometer. Next, 6 human subjects

underwent eyes-closed resting state EEG-fMRI with the MB sequence. EEG data quality was assessed by the ability to remove gradient and cardioballistic artifacts and a clean spectrogram.

Results

RF induced heating was lower at both electrodes in the MB sequence compared to the SB sequence at ratios of 0.7 and 0.8, respectively. These ratios are slightly greater than the ratio of RF power deposition of the sequences, which is 0.64. However, our results are consistent with the use of RF power deposition, characterized by B_1^+RMS, in predicting less heating in the MB sequence than the SB sequence. In the resting state EEG data, gradient and cardioballistic artifacts were successfully removed using traditional template subtraction. All subjects showed an individual alpha peak in the spectrogram with a posterior topography characteristic of eyes-closed EEG.

Conclusions

Our study shows that B_1^+RMS is a useful indication of the relative heating of fMRI protocols. This observation indicates that simultaneous EEG-fMRI recordings using this MB sequence can be safe in terms of RF-related heating, and that EEG data recorded using this sequence is of acceptable quality.

Introduction

As the technologies available to modern cognitive neuroscience advances, the access and practicality of utilizing multiple imaging modalities simultaneously has increased dramatically. Complimentary pairings of imaging techniques allows researchers a far more comprehensive view of the brain by overcoming the limitations of the individual modalities [1]. Simultaneously recorded electroencephalography (EEG) and functional magnetic resonance imaging (fMRI) are two such complimentary techniques; EEG offers high temporal resolution in the millisecond range while fMRI provides high spatial resolution in the order of mm^3, thus optimally capturing different types of neural activity [2]. Coupled with the non-invasive nature of recording and ease of access to equipment, the use of simultaneous EEG-fMRI is becoming more commonplace. The effectiveness of simultaneous EEG-fMRI has already been demonstrated for advancing the understanding of neuropsychiatric disorders [1], sleep [3–5], epilepsy [6,7], physiological rhythms [8], evoked activations [9–11], and ongoing brain activity and connectivity [12–14].

As a recent advance, concurrent EEG-fMRI imaging has begun to strongly benefit from simultaneous multi-band (MB) imaging in fMRI. In MB imaging multiple slices of the brain are acquired simultaneously. MB-fMRI offers higher temporal resolution than the traditional SB sequences at little cost to fMRI SNR [15]. MB sequences have been previously shown to have comparable, if not greater functional SNR than non-MB sequences [16–18]; this is facilitated by the greater sampling rate, or lower TR, which allows more acquisitions per unit time.

However, there are many technical challenges in acquiring high quality EEG-fMRI data, and little work has assessed how these challenges are further affected by the use of MB-fMRI sequences. The core challenge of concurrent recordings lies in the interaction between the EEG equipment and the fMRI scanner environment, causing artifacts in both modalities unique to simultaneous recordings. The

artifacts in fMRI are minor, comprising a small decrease in cortical signal-to-noise ratio (SNR) due to increases in static magnetic field inhomogeneities near the electrodes, but without significant effects on sensitivity to signal changes [19–22]. However, the acquired EEG data shows strong gradient artifacts (GA) produced by the magnet's gradient switching, ballistocardiographic (BCG) pulse artifacts caused by small movements of the body/electrodes due to cardiac pulsation combined with the Hall effect (production of a potential difference across an electrical conductor when a magnetic field is applied perpendicular to the flow of the current), and motion artifacts, especially in posterior electrodes [19,22]. A great deal of effort has been spent in the past two decades on the proper removal of these artifacts [22–27]. However, whether the methods previously developed to mitigate GA and BCG artifacts in concurrently recorded EEG are successful for newer MB-fMRI sequences is insufficiently investigated.

Previous investigations into quality of EEG recorded concurrently with MB-fMRI have demonstrated suitable data quality for several experimental conditions. Specifically, Foged et al. [19] found no adverse effects on data quality using MB factors 4 and 8 (TR of 450 and 280ms, respectively) and traditional GA and BCG artifact rejection methods. Uji et al. [28] used a silent recording paradigm, i.e. periods of active scanning interleaved with periods without active pulses (MB factor 3, TR=3000ms including 2,250ms silence). They showed that the EEG data acquired in the silent period was of high enough quality to investigate the EEG gamma frequency band that is otherwise particularly affected by the GA. Chen et al. [29] showed that compared to a SB sequence, a MB-fMRI sequence (MB factor 4, TR=550ms) had minimal differences in EEG channel variance and spectra, and improved statistical and spatial sensitivity for resting state fMRI scans with a lower scanning duration. However, the free parameters used in MB sequences change with the needs of individual experiments. Therefore, to establish the general feasibility of obtaining acceptable EEG quality concurrently with MB-fMRI it is critical to extend these few studies using other parameter sets optimized for other experimental needs. We chose our parameter set so as to scan the whole cerebrum at a short TR (MB factor 4, TR=440ms) without

83 exceeding an MB factor of 4, while sparing the EEG alpha frequency band (~8-12Hz) from residual RF
84 excitation repetition artifacts (appearing at 15.9Hz for our sequence, see methods).

85 More important than data quality when considering a new MB EEG-fMRI sequence is ensuring subject
86 safety. For EEG-fMRI the key safety concern is the deposition of radiofrequency (RF) power that causes
87 heating in the EEG leads and electrodes. While several studies have shown acceptable heating during
88 simultaneous EEG-fMRI with both standard and high-field magnets using conventional SB scanning
89 [20,30–32], only a few studies have demonstrated safe RF heating using MB EEG-fMRI [19,28,29,33],
90 making research into MB EEG-fMRI safety a critical necessity.

91 Electrode heating has previously been characterized as a function of the Specific Absorption Rate, SAR
92 [19,32]. However, the whole-body SAR estimates can differ amongst scanners [34,35], rely on
93 assumptions about the body being scanned [36], and typically provide biased measurements [34].
94 Given these problems it has been suggested to characterize safety limits using $B_1^{+}RMS$, which is a fixed
95 characteristic of the sequence and protocol and depends on the time-averaged RF amplitude
96 transmitted by the scanner [35]. $B_1^{+}RMS$ refers to the magnitude of the (positively rotating component
97 of the) oscillating magnetic field generated by the RF coil, and RMS refers to a root-mean-square, or
98 quadratic mean of the B_1 field calculated over time. This quantity is proportional to the oscillating
99 electric fields responsible for RF heating. The major manufacturer of in-bore EEG amplifiers, Brain
100 Products, has recently begun to use $B_1^{+}RMS$ to specify safety limits [37]. Because $B_1^{+}RMS$ is a relatively
101 new standard, its use to assess the safety of simultaneous fMRI-EEG has been limited to the most recent
102 literature on the safety of MB sequences [28].

103 The heating associated with a given experiment can be characterized in absolute or relative terms.
104 Absolute heating experiments attempt to measure the temperature change due to scanning for a given
105 experimental condition. The accuracy of these measurements is complicated by the presence of gradual

temperature drifts in the bore [19]. Because these drifts can cause considerable variability, multiple measurements are required to accurately quantify the small changes of temperature that occur during scanning [29].

By contrast, a relative measurement can be used to compare the heating of two sequences or protocols under identical experimental conditions, such as scanners, samples, and temperature drift of the bore [29]. Because these conditions will similarly affect both sequences, the ratio of heating will be relatively insensitive to them. If one of the sequences has been established as safe under a wide variety of experimental conditions, then the relative measurement can be used to show that a new sequence is likely to produce similar or less heating under a similar variety of conditions. Relative temperature measurements have the potential to isolate the scaling relationships that drive differences in heating between sequences. They have been used to show that for a wide variety of sequence types the heating increase linearly with RF deposition [32].

Most previous EEG-fMRI safety studies have reported the absolute heating of MB sequences during scanning [19,28,29]. The few reports that have included both MB and SB sequences have not related these differences to differences in $B_1^{+}RMS$ [19,29].

Here we measure the relative heating of a MB sequence compared to a SB sequence that has been established as safe under a wide variety of conditions [38]. We employ a novel experimental design in which we compensate for scanner drift by alternating between sequences multiple times. We compare the measured heating ratio with the heating ratio that is expected based on $B_1^{+}RMS$ values associated with the sequences.

Our experiments are performed using a MB-fMRI protocol chosen to exploit the ability of MB sequences to obtain images at high temporal resolution (low TR) without compromising image resolution or coverage. After demonstrating the safety of the protocol using a relative temperature measurement, we

demonstrate acceptable data quality using data obtained from human subjects during eyes-closed resting state. We evaluate the efficacy of GA and BCG artifact rejection using traditional artifact rejection methods and characteristics of the EEG power spectrum to determine acceptable EEG data quality.

METHODS

We completed two different experiments in this study; 1) a phantom recording for assessing electrode heating and safety using the MB sequence in simultaneous EEG-fMRI, and after establishing safety, 2) eyes-closed resting state recordings in human subjects utilizing simultaneous EEG-fMRI with the same MB sequence to assess EEG data quality.

Human subjects

Six subjects (four female) underwent two simultaneous EEG-fMRI sessions of eyes-closed resting state on two separate days (20 minutes total). They were instructed to avoid movement and stay awake. All subjects gave written informed consent according to procedures approved by the Institutional Review Board of the University of Illinois at Urbana-Champaign.

fMRI

MRI Equipment

Data were acquired on a 3 T Prisma scanner with a 64-channel head coil (Siemens, Erlangen, Germany). TR markers from the scanner used for EEG-fMRI artifact removal were relayed through a specialized

hardware box, the RTBox [39], connected directly to the scanner. Scanner clock synchronization was achieved using a BrainProducts SyncBox (Gilching, Germany) connected directly via a cable to the scanner's 10 MHz clock.

MRI Sequences

Anatomical information was obtained using a high-resolution 3D structural MPRAGE scan (0.9 mm isotropic, TR: 1900 ms, TI: 900 ms, TE = 2.32 ms, GRAPPA factor = 2).

Our MB protocol was chosen to minimize TR, while still maintaining the resolution and coverage typically used for non-MB sequences. The parameters of the MB protocol were: TR: 440 ms, TE: 25 ms, flip angle: 40°, 28 slices, MB factor: 4, excitation pulse duration: 5300 us, GRAPPA acceleration factor: 2, slice thickness: 3.5 mm, fat saturation: on, bandwidth: 2056 Hz per pixel, in-plane resolution: 128 x 128, FoV: 230x230mm, voxel size: 1.8x1.8x3.5mm. Our laboratory has a particular interest in alpha band oscillations to address cognitive neuroscience questions [12,40,41]. Therefore, the MB factor and slice number were chosen to maintain maximal brain coverage at a short TR while moving the RF excitation repetition artifact outside of the traditional EEG alpha band range (~8-12Hz). Seven RF pulses (28 slices / MB factor 4 = 7) every 440ms corresponds to an RF excitation repetition at 15.9Hz, which is well above the alpha frequency range. A decrease in TR will increase SAR deposition for a fixed number of RF excitations; however, we compensated for this effect by using a relatively low flip angle of 40° and relatively long excitation pulse duration of 5300 µs. The use of low flip angles, even significantly lower than the Ernst angle, is not expected to negatively impact functional contrast [42].

We validated that this protocol had sufficient functional contrast-to-noise ratio, by comparing it against a SB sequence optimized for brain coverage, which we name SB-COV (TR: 1800 ms, TE: 25 ms, flip angle:

90, 34 slices, slice thickness 3 mm, fat saturation on, GRAPPA acceleration factor: 2, bandwidth: 2470 Hz per pixel, resolution: 92 x 92, FoV: 230x230mm). A single pilot subject ran through a functional localizer task designed to identify auditory-, face-, and object-processing areas for each imaging sequence. The localizer consisted of two tasks, first a passive listening task to target auditory areas [43], followed by a 1-back task using randomized blocks of Ekman faces [44] and household objects to target face-specific [45] and object-specific [46] areas, respectively (15 trials per block, 9 emotion blocks equally split between sad/angry/neutral expressions, and 3 object blocks). FMRI data was preprocessed and analyzed in MATLAB 2018b [47] using SPM12 (revision 7487) [48]. Preprocessing included realignment, co-registration, normalization to MNI stereotactic space, and smoothing (FWHM=6mm). The contemporary SB-COV sequence additionally underwent slice time correction prior to realignment. As expected in accord with prior evidence, for all three contrasts, the MB sequence demonstrated increased functional contrast-to-noise ratio (Fig 1). Considering the robust prior evidence [16,17], the current demonstration in a single subject should be considered a confirmatory proof of principle.

Fig 1. Comparison of functional activations in a localizer task between the MB sequence and the SB-COV sequence.

The visualized contrasts correspond to sounds>implicit baseline (A), faces>objects (B), and objects>faces (C) (threshold for visualization purposes: voxel-wise p<0.001 uncorrected). For each contrast, top and bottom rows (MB and SB-COV sequence, respectively) show equivalent slices for comparison. Activations comparable or stronger for the MB sequence are observed at the auditory cortex (A), the fusiform face area (B), and lateral occipital object-specific areas (C).

196 Heating experiment: To examine electrode heating via RF power deposition, we compared the MB
197 sequence against a sequence chosen to comply with the maximum intensity limits recommended by the
198 manufacturer of the EEG equipment (Brain Products; [38]), which we name SB-RF. The parameters of
199 SB-RF were TR: 2000 ms, TE: 30 ms, flip angle: 90, 25 slices, slice thickness 4 mm, fat saturation: on,
200 bandwidth: 2470 Hz, resolution: 92 x 92, FoV: 230x230mm. For the MB protocol B_1^+RMS was 0.8 µT;
201 whereas B_1^+RMS of the SB-RF protocol was 1.0 µT. Because RF energy deposition scales as the square
202 of B_1^+ [49], the MB sequence is expected to exhibit lower RF energy deposition than the SB-RF protocol
203 by a factor of $(8/10)^2$ =0.64. This estimate is in line with time-averaged RF power deposition values
204 reported by the scanner during scanning of a standard 2 liter aqueous Siemens phantom designed to
205 mimic typical body coil loading: 3.2 for the MB protocol and 5.0 for the SB-RF, with the ratio being
206 3.2/5.0 = 0.64. Given that the heating scales with the RF power deposition, it is expected that heating
207 during the MB protocol will be lower than that of the SB-RF protocol by a factor of 0.64.
208
209 EEG data quality experiment: Using the MB protocol we obtained fMRI data with simultaneous EEG from
210 6 human subjects during two eyes-closed resting state sessions of 10 minutes each as part of a larger
211 experiment using the MB sequence.
212
213 ***EEG data acquisition***
214 *EEG Equipment and Setup*
215 EEG data was recorded with a 64-channel EEG cap in the standard 10-10-20 montage from
216 BrainProducts that included 61 scalp electrodes and 3 drop-down electrodes (HEOG, IO, ECG) using the
217 manufacturer's BrainVision Recorder software (BrainVision Recorder; [50]). The cap was connected to
218 two MR-compatible BrainVision 32-channel EEG amplifiers within the scanner bore, and all impedances

were kept <5 kOhms. For all scans using EEG-fMRI the amplifiers and battery pack were strapped down and sandbagged to a stabilizing sled from BrainProducts to reduce vibration artifacts. The EEG recording hardware was directly connected to the SyncBox, which was also connected to the MR clock signal, producing 'Sync On' markers to verify synchronization. The RTBox was directly connected to the scanner and placed scanner pulse markers in the EEG file at the time of delivery of every RF pulse. The scalp electrodes had 10 kOhm built-in resistors (5 at amplifier + 5 at tip) and were recorded with a 0.5 µV resolution. The drop-down electrodes had 20 kOhm built-in resistors (5 at amplifier + 15 at tip) and were recorded with a 10 µV resolution. All electrodes had a low cutoff filter of 10s, high cutoff filter of 250Hz, and a sampling rate of 5000Hz. This combination of microvolt resolutions, sampling rate, and cutoffs gave us the highest possible recording resolution while avoiding amplifier overloading. Preventing overloading of the amplifiers is critical for EEG-fMRI to ensure that the peaks of the artifact can be detected for GA/BCG artifact rejection. Additionally, during all human subject runs the scanner's helium pump was turned off to eliminate vibration artifacts at 42 Hz from the pump.

During the electrode heating tests a watermelon 'phantom' was fit with the 64-channel cap and left to equilibrate in the scanner bore overnight. The watermelon provides a conductive surface and permits fine-grained control over impedances at electrode contacts [29,51]. We abraded the watermelon with sandpaper prior to placing the cap on it and applying electrolytic gel to the electrodes, which allowed us to maintain impedances <5 kOhm, thereby protect the amplifiers from high voltages induced by the scanner. Given the small size of the watermelon, the ECG electrode was routed underneath the watermelon once and placed in between the HEOG and IOG electrodes to ensure that no loop was created within the magnet (Fig 2).

Fig 2. Watermelon 'phantom' outfitted with the 64-channel BrainProducts EEG cap.

Using a watermelon as phantom provides a conductive surface and permits fine-grained control over impedances at electrode contacts. Thermometers are attached to the ECG and TP7 electrodes. The ECG electrode was wrapped underneath the watermelon to prevent the wire from forming a loop. Prior to the heating experiment the watermelon was left in the scanner bore overnight to equilibrate and then abraided with sandpaper to achieve safe impedances.

EEG Data Processing

EEG data was preprocessed using the BrainVision Analyzer software (Version 2.2) [52]. Following standard procedures, GA subtraction was performed first followed by BCG artifact rejection as first done by Allen et. al [23,53]. The GA subtraction used marker detection from the trigger pulse markers obtained directly from the scanner (see methods) with a continuous artifact. A baseline correction over the whole artifact was used with a sliding average calculation of 21 marker intervals. Bad intervals were corrected with the average of all channels. The data was not downsampled (to minimize preprocessing). A lowpass FIR filter was applied at 100 Hz. The data was then segmented to include only artifact-free resting-state data, and BCG artifact rejection was performed using semi-automatic mode. After correcting all marked heartbeats, artifact removal of the heartbeat template was performed using sequential 21 pulse templates as the template average.

EEG data were analyzed in MATLAB 2018b [47] using EEGLAB (Version 2019.1) [54]. Prior to spectral analysis, the data was passed through a second lowpass FIR filter at 70 Hz. The spectrograms for scalp channels of each subject were computed at a frequency resolution of 0.2 Hz using the Multitaper approach. We chose not to do any further processing of the data (i.e., ICA decomposition) as we wanted

264 to show the quality of the data with the minimum amount of cleaning resulting from the BrainVision
265 Analyzer artifact rejections.

266

267 ***Heating probes***

268 Temperature changes during scanning were measured with a Luxtron 812 two channel fluoroptic
269 thermometer (LumaSense Technologies, Ballerup, Denmark). Fluoroptic probes were placed in the
270 conductive paste between the electrodes and the watermelon surface. One of the probes was placed
271 beneath the ECG electrode, because this electrode has the longest leads and is therefore expected to
272 exhibit greater heating [55]. The second probe was placed beneath the TP7 electrode because it is close
273 to the rungs of the head coil and has one of longest leads of the electrode caps.

274 Heating during the MB sequence was compared against the SB-RF protocol. This was done by running
275 each sequence three times, in an alternating fashion. Each of the runs consisted of approximately 13.5
276 minutes of scanning and were spaced by approximately 5 minutes of rest between scans. The purpose of
277 alternating the scans was to minimize bias due to long-term drift of the temperature. During the
278 experiment, the fluoroptic thermometer performed two measurements per second; data were recorded
279 by a computer connected to the Luxtron unit via a serial cable. Temperature signals were smoothed
280 with a Gaussian filter using a window size of 200 seconds. To quantify heating during each scan we
281 calculated the difference in the smoothed temperature between the onset of the scan and the end of
282 the scan. This value was divided by the scan duration to calculate an average rate of heating. For each
283 electrode and sequence combination, the three heating rate measurements were averaged.

284

285 **RESULTS**

286 ***Relative heating of the MB sequences vs. SB-RF***

287 To assure the safety of our MB sequence, we aimed at demonstrating that heating at EEG electrodes
288 remained below that of the recommended SB sequence previously established to be safe [38]. The
289 temperature of the ECG electrode steadily increased over the course of the experiment, as shown in Fig
290 3A. Superposition of the temperature changes during each of the scans reveal consistently greater
291 heating of the SB-RF protocol, as shown in Fig 3B. The average rate of heating for the MB protocol was
292 lower than that of the SB-RF protocol SB-RF protocol by a factor of 0.7, as shown in Table 1. The
293 measured heating differences between the two sequences therefore is in approximate agreement with
294 the RF power deposition ratio of 0.64 derived from the scanner (see Methods). This implies that the
295 differences in heating between the two sequences are captured by the total RF power deposition.
296 Because the empirically measured heating was below that of the safe SB-RF sequence, our MB sequence
297 can be considered to be safe.

298

299 ***Fig 3. Temperature measurements at the ECG electrode during the MB sequence (red) and the SB-RF***
300 ***sequence (blue).***

301 *(A) Temperature change over the total course of the experiment. Black lines denote rest periods of no*
302 *scanning. (B) The heating curves of the individual runs are superimposed.*

303

304 **Table 1. Comparison of heating of the MB and SB-RF protocols at the ECG and the TP7 electrodes.**

	ECG electrode	TP7 electrode
MB, Heating rate (degrees/min)	0.015	0.011
SB-RF, Heating rate (degrees/min)	0.021	0.014
MB/SB-RF, ratio of heating rates	0.7	0.8

The temperature of the TP7 electrode also steadily increased over the course of the experiment, as shown in Fig 4A. The temperature increase persisted during the rest periods during which no scanning was performed, indicating temperature drift, likely due to changes in the temperature of the environment. Superposition of the temperature changes during each of the scans revealed similar heating for the two sequences, except for one of the SB-RF scans which showed greater heating, as shown in Fig. 4B. The average rate of heating for the MB protocol was lower than that of the SB-RF protocol by a factor of 0.8, as shown in Table 1. Because the empirically measured heating in TP7 was likewise below or similar to that of the safe SB-RF sequence, our MB sequence can be considered to be safe.

Fig 4. Temperature measurements at the TP7 electrode during the MB sequence (red) and the SB-RF sequence (blue).

(A) Temperature change over the total course of the experiment. Black lines denote rest periods of no scanning. (B) The heating curves of the individual runs are superimposed.

EEG Data quality validation

To check EEG signal quality, we assessed the spectral dominance and topography of the alpha frequency band upon GA and BCG artifact cleaning. Alpha-band oscillations are uniquely positioned for this purpose because their exceptionally high power rises above the 1/f aperiodic component of the EEG spectrum during eyes-closed resting state. Fig 5 shows the log-power spectrogram of the EEG during eyes-closed resting state in a single subject (Subject 2). We demonstrate that each successive step

327 substantially improves data quality, first showing the raw data without GA or BCG artifact subtraction
328 (Fig 5A), then with only the GA artifact cleaned (Fig 5B), and finally the fully cleaned data with both GA
329 and BCG artifacts removed (Fig 5C).The cleaned spectrogram showed a clear power peak in the alpha
330 range (~10Hz) as expected during relaxed eyes-closed states, while displaying only a minimal residual
331 power increase related to the GA at the RF excitation repetition frequency (Fig 5D). Fig 6a shows the log-
332 power spectrum for each of 6 subjects averaged across posterior electrodes (O1, O2, Oz, PO3, PO4, PO7,
333 PO8, POz) typically capturing particularly high power in the alpha range. For each subject we determined
334 the individual alpha peak frequency at which power was highest in the ~8-12 Hz range [56] (denoted by
335 a star for each subject in Fig 6A). At each subject's individual alpha peak frequency, a posterior
336 topography (derived from all channels) was detectable in all individual subjects (Fig 6B), while other
337 power peaks in lower frequencies (particularly vulnerable to BCG artifacts) or at 15.9 Hz (the RF
338 excitation repetition frequency) were greatly attenuated. We conclude that EEG is of sufficient quality
339 for cognitive neuroscience research after application of artifact rejection methods originally developed
340 for SB sequences, specifically template subtraction [23,53].

341

342 ***Fig 5. Log-power spectrogram of the EEG during eyes-closed resting state in a single subject during***
343 ***concurrent fMRI recordings with the MB sequence.***

344 *The spectrogram is shown for the (A) raw EEG data without artifact removal, (B) the EEG data with GA*
345 *artifact rejected but prior to BCG correction, and (C) the cleaned EEG data after both GA and BCG artifact*
346 *correction. Each trace corresponds to one of 60 scalp channels (1 excluded due to excessive noise). (D)*
347 *shows the scalp topography at 10Hz for the cleaned EEG data. The prominent power peak at ~10Hz*
348 *emerging more clearly after artifact correction (in C) and the posterior topography (in D) are consistent*

with the spectral dominance of the alpha rhythm in eyes-closed resting state. The dotted line represents the frequency of the RF repetition artifact at 15.9 Hz. This subject corresponds to Subject 2 in Fig 6.

Fig 6. EEG log-power spectrogram and topographies during eyes-closed resting state for all human subjects during concurrent fMRI recordings with the MB sequence.

(A) Power spectral density averaged across 8 posterior channels of each subject (O1, O2, Oz, PO3, PO4, PO7, PO8, POz). The stars denote the individual subjects' maximum values within the alpha band (8-12 Hz) i.e. individual alpha peak. The dotted line represents the scanner artifact at 15.9 Hz. (B) Corresponding scalp topographies using all channels for the 6 subjects at the individual alpha peak frequency.

Discussion

Simultaneously recorded EEG-fMRI is a powerful tool that can provide information beyond what unimodal approaches are able to [57–59]. Although EEG-fMRI using traditional SB sequences is fairly well established, EEG-fMRI imaging using modern MB fMRI sequences lacks similar safety and data quality guidelines. Here we demonstrate that a particular MB sequence with high temporal resolution (440ms TR) produces less RF heating at the EEG electrode sites than a traditional EPI sequence while maintaining acceptable EEG data quality.

Although previous studies have compared heating of a MB sequence with that of SB sequences [19,29], our study employs an interleaved strategy designed to minimize the effect of temperature drift so as to accurately characterize the relative heating. This strategy is important for confirming the usefulness of $B_1^{\dagger}RMS$ to quantify the relative heating of these sequences.

371 Based on scanner-reported values of B_1^+RMS and time-averaged RF power deposition, we expected that
372 heating during our MB protocol to be lower than that of the SB-RF protocol by a factor of 0.64. We
373 empirically measured heating ratios of 0.7 and 0.8 in the ECG and TP7 electrodes, respectively.
374 Therefore, the heating associated with the MB sequence was less than that of the SB-RF, as expected.
375 Our measured heating ratios are slightly greater than the expected ratio. This is likely due to the
376 presence of experimental noise, which tends to cause the measured heating ratio to approach unity.
377 Experimental noise arises from limitations in the precision of the fluoroptic thermometer, and from
378 variability between scans.

379 In absolute terms, the heating rates we measured for all conditions were greater than 0.01 degrees
380 C/min (see Table 1). These rates are higher than those observed in similar experiments [19]. This is likely
381 due to a positive drift in the bore temperature, which is apparent during the rest periods observed in Fig
382 4. These observations underscore the fact that temperature drifts are a serious complication for
383 measuring the effect of scanning on absolute heating. Our results also demonstrate the potential of a
384 relative measurement to compensate for drift, and the value of alternating between sequences multiple
385 times while performing such measurements.

386 We observed a greater temperature increase for the ECG electrode than for the TP7 electrode. This
387 difference is likely because the ECG electrode has the longest lead. Moreover, unlike human
388 experiments, the use of our phantom required the formation of a partial loop, which may have further
389 boosted the heating [30]. These amplifications of the heating signal may have been beneficial for a more
390 accurate detection of the relative heating between the two protocols. For TP7, any amplification of the
391 heating signal would have been less pronounced, causing the differences between sequences to be
392 more difficult to detect and causing the measured heating ratio of TP7 to be closer to unity than that of
393 the ECG electrode. Future investigation is required to demonstrate whether a partial loop can be used
394 to improve the precision of relative heating experiments.

Our results support the usefulness of $B_1^{+}RMS$ as a benchmark for assessing protocol safety. We have shown that values of $B_1^{+}RMS$ can be maintained at acceptable levels even when using a MB factor of 4, a low TR of 440 ms, and 28 slices for whole-cerebrum coverage. This was achieved by using a relatively low flip angle of 40°, and a moderately long pulse duration of 5300 µs.

In addition to verifying heating safety, in our second experiment we conducted preliminary investigations into the success of GA and BCG artifact rejection for the EEG data acquired concurrently with our MB sequence. To this end, we assessed the spectral dominance and topography of the alpha frequency band due to its uniquely high and easily identifiable power during eyes-closed resting state. Indeed, after GA and BCG artifact rejection a clear posterior topography at a readily identifiable individual alpha peak frequency was observed in all six human subjects. Of note, due to our research interest in alpha oscillations [41] we chose the RF excitation frequency so as to spare this band from potential residual GA artifacts (see Methods). Particularly important, we saw the power at the RF excitation repetition frequency greatly attenuated after artifact rejection, implying that noise generated by the MRI sequence is not dominating the signal. Our observations in the EEG power spectrum indicate that traditional MR artifact rejection techniques [23,53] are sufficient for use in MB EEG-fMRI recordings. Future work would include more explicit comparisons of concurrently recorded EEG data quality between MB, SB, and scanner-off recordings.

To conclude, our results confirm the usefulness of $B_1^{+}RMS$ in characterizing the relative heating of fMRI sequences. This work adds additional support to the growing body of literature on the safety and efficacy of multiband simultaneous EEG-fMRI imaging.

415 **References**

416 1. Liu S, Cai W, Liu S, Zhang F, Fulham M, Feng D, et al. Multimodal neuroimaging computing: a
417 review of the applications in neuropsychiatric disorders. Brain Inform. 2015;2: 167–180.
418 doi:10.1007/s40708-015-0019-x

419 2. Hari R, Parkkonen L. The brain timewise: how timing shapes and supports brain function. Philos
420 Trans R Soc Lond B Biol Sci. 2015;370. doi:10.1098/rstb.2014.0170

421 3. Duyn JH. EEG-fMRI Methods for the Study of Brain Networks during Sleep. Front Neurol. 2012;3.
422 doi:10.3389/fneur.2012.00100

423 4. Fang Z, Ray LB, Owen AM, Fogel SM. Brain Activation Time-Locked to Sleep Spindles Associated
424 With Human Cognitive Abilities. Frontiers in Neuroscience. 2019;13. doi:10.3389/fnins.2019.00046

425 5. Laufs H, Walker MC, Lund TE. 'Brain activation and hypothalamic functional connectivity during
426 human non-rapid eye movement sleep: an EEG/fMRI study'--its limitations and an alternative
427 approach. Brain. 2007;130: e75–e75. doi:10.1093/brain/awm084

428 6. Gotman J, Kobayashi E, Bagshaw AP, Bénar C-G, Dubeau F. Combining EEG and fMRI: A multimodal
429 tool for epilepsy research. Journal of Magnetic Resonance Imaging. 2006;23: 906–920.
430 doi:10.1002/jmri.20577

431 7. Gotman J. Epileptic networks studied with EEG-fMRI. Epilepsia. 2008;49: 42–51.
432 doi:10.1111/j.1528-1167.2008.01509.x

433 8. Tyvaert L, LeVan P, Grova C, Dubeau F, Gotman J. Effects of fluctuating physiological rhythms
434 during prolonged EEG-fMRI studies. Clin Neurophysiol. 2008;119: 2762–2774.
435 doi:10.1016/j.clinph.2008.07.284

9. Bénar C-G, Schön D, Grimault S, Nazarian B, Burle B, Roth M, et al. Single-trial analysis of oddball event-related potentials in simultaneous EEG-fMRI. Human Brain Mapping. 2007;28: 602–613. doi:10.1002/hbm.20289

10. Walz JM, Goldman RI, Carapezza M, Muraskin J, Brown TR, Sajda P. Simultaneous EEG-fMRI Reveals a Temporal Cascade of Task-Related and Default-Mode Activations During a Simple Target Detection Task. Neuroimage. 2014;102: 229–239. doi:10.1016/j.neuroimage.2013.08.014

11. Rusiniak M, Lewandowska M, Wolak T, Pluta A, Milner R, Ganc M, et al. A modified oddball paradigm for investigation of neural correlates of attention: a simultaneous ERP–fMRI study. MAGMA. 2013;26: 511–526. doi:10.1007/s10334-013-0374-7

12. Sadaghiani S, Scheeringa R, Lehongre K, Morillon B, Giraud A-L, Kleinschmidt A. Intrinsic Connectivity Networks, Alpha Oscillations, and Tonic Alertness: A Simultaneous Electroencephalography/Functional Magnetic Resonance Imaging Study. Journal of Neuroscience. 2010;30: 10243–10250. doi:10.1523/JNEUROSCI.1004-10.2010

13. Wirsich J, Giraud A-L, Sadaghiani S. Concurrent EEG- and fMRI-derived functional connectomes exhibit linked dynamics. NeuroImage. 2020;219: 116998. doi:10.1016/j.neuroimage.2020.116998

14. Chang C, Liu Z, Chen MC, Liu X, Duyn JH. EEG correlates of time-varying BOLD functional connectivity. NeuroImage. 2013;72: 227–236. doi:10.1016/j.neuroimage.2013.01.049

15. Feinberg DA, Setsompop K. Ultra-Fast MRI of the Human Brain with Simultaneous Multi-Slice Imaging. J Magn Reson. 2013;229: 90–100. doi:10.1016/j.jmr.2013.02.002

16. Demetriou L, Kowalczyk OS, Tyson G, Bello T, Newbould RD, Wall MB. A comprehensive evaluation of increasing temporal resolution with multiband-accelerated protocols and effects on statistical

457 outcome measures in fMRI. NeuroImage. 2018;176: 404–416.
458 doi:10.1016/j.neuroimage.2018.05.011

459 17. Todd N, Moeller S, Auerbach EJ, Yacoub E, Flandin G, Weiskopf N. Evaluation of 2D multiband EPI
460 imaging for high-resolution, whole-brain, task-based fMRI studies at 3T: Sensitivity and slice
461 leakage artifacts. NeuroImage. 2016;124: 32–42. doi:10.1016/j.neuroimage.2015.08.056

462 18. Glasser MF, Smith SM, Marcus DS, Andersson J, Auerbach EJ, Behrens TEJ, et al. The Human
463 Connectome Project's Neuroimaging Approach. Nat Neurosci. 2016;19: 1175–1187.
464 doi:10.1038/nn.4361

465 19. Foged MT, Lindberg U, Vakamudi K, Larsson HBW, Pinborg LH, Kjær TW, et al. Safety and EEG data
466 quality of concurrent high-density EEG and high-speed fMRI at 3 Tesla. PLoS One. 2017;12.
467 doi:10.1371/journal.pone.0178409

468 20. Carmichael DW, Thornton JS, Rodionov R, Thornton R, McEvoy AW, Ordidge RJ, et al. Feasibility of
469 simultaneous intracranial EEG-fMRI in humans: A safety study. NeuroImage. 2010;49: 379–390.
470 doi:10.1016/j.neuroimage.2009.07.062

471 21. Luo Q, Glover GH. Influence of Dense Array EEG Cap on fMRI Signal. Magn Reson Med. 2012;68:
472 807–815. doi:10.1002/mrm.23299

473 22. Mullinger KJ, Castellone P, Bowtell R. Best Current Practice for Obtaining High Quality EEG Data
474 During Simultaneous fMRI. J Vis Exp. 2013 [cited 12 Jun 2020]. doi:10.3791/50283

475 23. Allen PJ, Josephs O, Turner R. A Method for Removing Imaging Artifact from Continuous EEG
476 Recorded during Functional MRI. NeuroImage. 2000;12: 230–239. doi:10.1006/nimg.2000.0599

24. Grouiller F, Vercueil L, Krainik A, Segebarth C, Kahane P, David O. A comparative study of different artefact removal algorithms for EEG signals acquired during functional MRI. NeuroImage. 2007;38: 124–137. doi:10.1016/j.neuroimage.2007.07.025

25. Ihalainen T, Kuusela L, Turunen S, Heikkinen S, Savolainen S, Sipilä O. Data quality in fMRI and simultaneous EEG–fMRI. Magn Reson Mater Phy. 2015;28: 23–31. doi:10.1007/s10334-014-0443-6

26. Daniel AJ, Smith JA, Spencer GS, Jorge J, Bowtell R, Mullinger KJ. Exploring the relative efficacy of motion artefact correction techniques for EEG data acquired during simultaneous fMRI. Human Brain Mapping. 2019;40: 578–596. doi:10.1002/hbm.24396

27. Luo Q, Huang X, Glover GH. Ballistocardiogram artifact removal with a reference layer and standard EEG cap. Journal of Neuroscience Methods. 2014;233: 137–149. doi:10.1016/j.jneumeth.2014.06.021

28. Uji M, Wilson R, Francis ST, Mullinger KJ, Mayhew SD. Exploring the advantages of multiband fMRI with simultaneous EEG to investigate coupling between gamma frequency neural activity and the BOLD response in humans. Human Brain Mapping. 2018;39: 1673–1687. doi:10.1002/hbm.23943

29. Chen JCC, Forsyth A, Dubowitz DJ, Muthukumaraswamy SD. On the Quality, Statistical Efficiency, and Safety of Simultaneously Recorded Multiband fMRI/EEG. Brain Topogr. 2020;33: 303–316. doi:10.1007/s10548-020-00761-w

30. Lemieux L, Allen PJ, Franconi F, Symms MR, Fish DK. Recording of EEG during fMRI experiments: Patient safety. Magnetic Resonance in Medicine. 1997;38: 943–952. doi:10.1002/mrm.1910380614

31. Jorge J, Grouiller F, Ipek Ö, Stoermer R, Michel CM, Figueiredo P, et al. Simultaneous EEG–fMRI at ultra-high field: Artifact prevention and safety assessment. NeuroImage. 2015;105: 132–144. doi:10.1016/j.neuroimage.2014.10.055

32. Nöth U, Laufs H, Stoermer R, Deichmann R. Simultaneous electroencephalography-functional MRI at 3 T: An analysis of safety risks imposed by performing anatomical reference scans with the EEG equipment in place. Journal of Magnetic Resonance Imaging. 2012;35: 561–571. doi:10.1002/jmri.22843

33. Kyathanahally SP, Wang Y, Calhoun VD, Deshpande G. Investigation of True High Frequency Electrical Substrates of fMRI-Based Resting State Networks Using Parallel Independent Component Analysis of Simultaneous EEG/fMRI Data. Front Neuroinform. 2017;11. doi:10.3389/fninf.2017.00074

34. Baker KB, Tkach JA, Nyenhuis JA, Phillips M, Shellock FG, Gonzalez-Martinez J, et al. Evaluation of specific absorption rate as a dosimeter of MRI-related implant heating. Journal of Magnetic Resonance Imaging. 2004;20: 315–320. doi:10.1002/jmri.20103

35. Faulkner W. New MRI Safety Labels & Devices. Signals. 2016;5. Available: https://www.ismrm.org/smrt/E-Signals/2016FEBRUARY/eSig_5_1_hot_2.htm

36. Nitz WR, Brinker G, Diehl D, Frese G. Specific Absorption Rate as a Poor Indicator of Magnetic Resonance-Related Implant Heating. Investigative Radiology. 2005;40: 773–776. doi:10.1097/01.rli.0000185898.59140.91

37. Warbrick T. Exciting news for our EEG-fMRI customers: Update of MRI sequence conditions. Brain Products GmbH. Apr 2020Products&Applications.

38. Brain Products. BrainAmp MR: Operating Instructions for use in an MR environment. 014 ed. Gilching, Germany; 2012.

39. Li X, Liang Z, Kleiner M, Lu Z-L. RTbox: A device for highly accurate response time measurements. Behavior Research Methods. 2010;42: 212–225. doi:10.3758/BRM.42.1.212

40. Sadaghiani S, Scheeringa R, Lehongre K, Morillon B, Giraud A-L, D'Esposito M, et al. Alpha-Band Phase Synchrony Is Related to Activity in the Fronto-Parietal Adaptive Control Network. Journal of Neuroscience. 2012;32: 14305–14310. doi:10.1523/JNEUROSCI.1358-12.2012

41. Sadaghiani S, Kleinschmidt A. Brain Networks and α-Oscillations: Structural and Functional Foundations of Cognitive Control. Trends in Cognitive Sciences. 2016;20: 805–817. doi:10.1016/j.tics.2016.09.004

42. Gonzalez-Castillo J, Roopchansingh V, Bandettini PA, Bodurka J. Physiological noise effects on the flip angle selection in BOLD fMRI. NeuroImage. 2011;54: 2764–2778. doi:10.1016/j.neuroimage.2010.11.020

43. Sadaghiani S, Hesselmann G, Kleinschmidt A. Distributed and Antagonistic Contributions of Ongoing Activity Fluctuations to Auditory Stimulus Detection. Journal of Neuroscience. 2009;29: 13410–13417. doi:10.1523/JNEUROSCI.2592-09.2009

44. Ekman P, Friesen W. Pictures of Facial Affect. Palo Alto, CA: Consulting Psychologists Press; 1976.

45. Berman MG, Park J, Gonzalez R, Polk TA, Gehrke A, Knaffla S, et al. Evaluating Functional Localizers: The Case of the FFA. Neuroimage. 2010;50: 56–71. doi:10.1016/j.neuroimage.2009.12.024

46. Grill-Spector K, Kourtzi Z, Kanwisher N. The lateral occipital complex and its role in object recognition. Vision Research. 2001;41: 1409–1422. doi:10.1016/S0042-6989(01)00073-6

539 47. MATLAB. Version 9.5.0.944444 (R2018b). Natick, MA: The MathWorks Inc.; 2018.

540 48. Penny W, Friston K, Ashburner J, Kiebel S, Nichols T. Statistical Parametric Mapping: The Analysis
541 of Functional Brain Images. 1st ed. Cambridge, MA: Academic Press; 2006.

542 49. Bernstein M, King K, Zhou X. Introduction to Radiofrequency Pulses. 1st ed. Handbook of MRI Pulse
543 Sequences. 1st ed. Cambridge, MA: Academic Press; 2004. pp. 29, 31–34.

544 50. Brain Products. BrainVision Recorder 1.20: User Manual. 007 ed. Gilching, Germany; 2012.

545 51. Balasubramanian M, Wells WM, Ives JR, Britz P, Mulkern RV, Orbach DB. RF Heating of Gold Cup
546 and Conductive Plastic Electrodes during Simultaneous EEG and MRI. Neurodiagn J. 2017;57: 69–
547 83. doi:10.1080/21646821.2017.1256722

548 52. Brain Products. BrainVision Analyzer V. 2.0.2: User Manual. 004 ed. Gilching, Germany; 2012.

549 53. Allen PJ, Polizzi G, Krakow K, Fish DR, Lemieux L. Identification of EEG Events in the MR Scanner:
550 The Problem of Pulse Artifact and a Method for Its Subtraction. NeuroImage. 1998;8: 229–239.
551 doi:10.1006/nimg.1998.0361

552 54. Delorme A, Makeig S. EEGLAB: an open source toolbox for analysis of single-trial EEG dynamics
553 including independent component analysis. Journal of Neuroscience Methods. 2004;134: 9–21.
554 doi:10.1016/j.jneumeth.2003.10.009

555 55. Angelone LM, Potthast A, Segonne F, Iwaki S, Belliveau JW, Bonmassar G. Metallic electrodes and
556 leads in simultaneous EEG-MRI: Specific absorption rate (SAR) simulation studies.
557 Bioelectromagnetics. 2004;25: 285–295. doi:10.1002/bem.10198

558 56. Klimesch W. EEG alpha and theta oscillations reflect cognitive and memory performance: a review
559 and analysis. Brain Research Reviews. 1999;29: 169–195. doi:10.1016/S0165-0173(98)00056-3

560 57. Ritter P, Villringer A. Simultaneous EEG–fMRI. Neuroscience & Biobehavioral Reviews. 2006;30:
561 823–838. doi:10.1016/j.neubiorev.2006.06.008

562 58. Calhoun VD, Sui J. Multimodal fusion of brain imaging data: A key to finding the missing link(s) in
563 complex mental illness. Biol Psychiatry Cogn Neurosci Neuroimaging. 2016;1: 230–244.
564 doi:10.1016/j.bpsc.2015.12.005

565 59. Sadaghiani S, Wirsich J. Intrinsic connectome organization across temporal scales: New insights
566 from cross-modal approaches. Netw Neurosci. 2020;4: 1–29. doi:10.1162/netn_a_00114

567

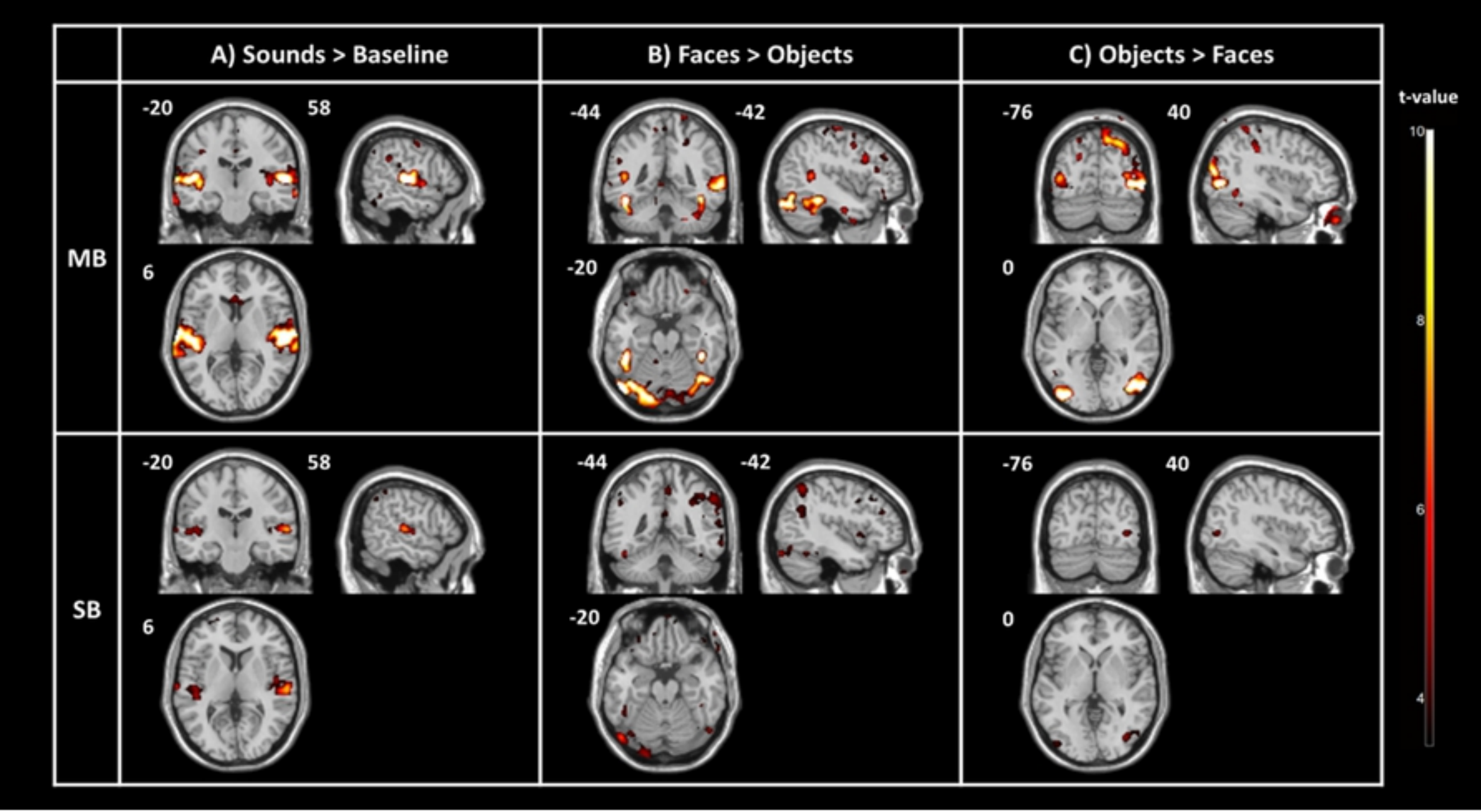
A) Sounds > Baseline
B) Faces > Objects
C) Objects > Faces
MB
SB
-20
58
6
-44
-42
-20
-76
40
0
t-value
10
8
6
4

Figure 1

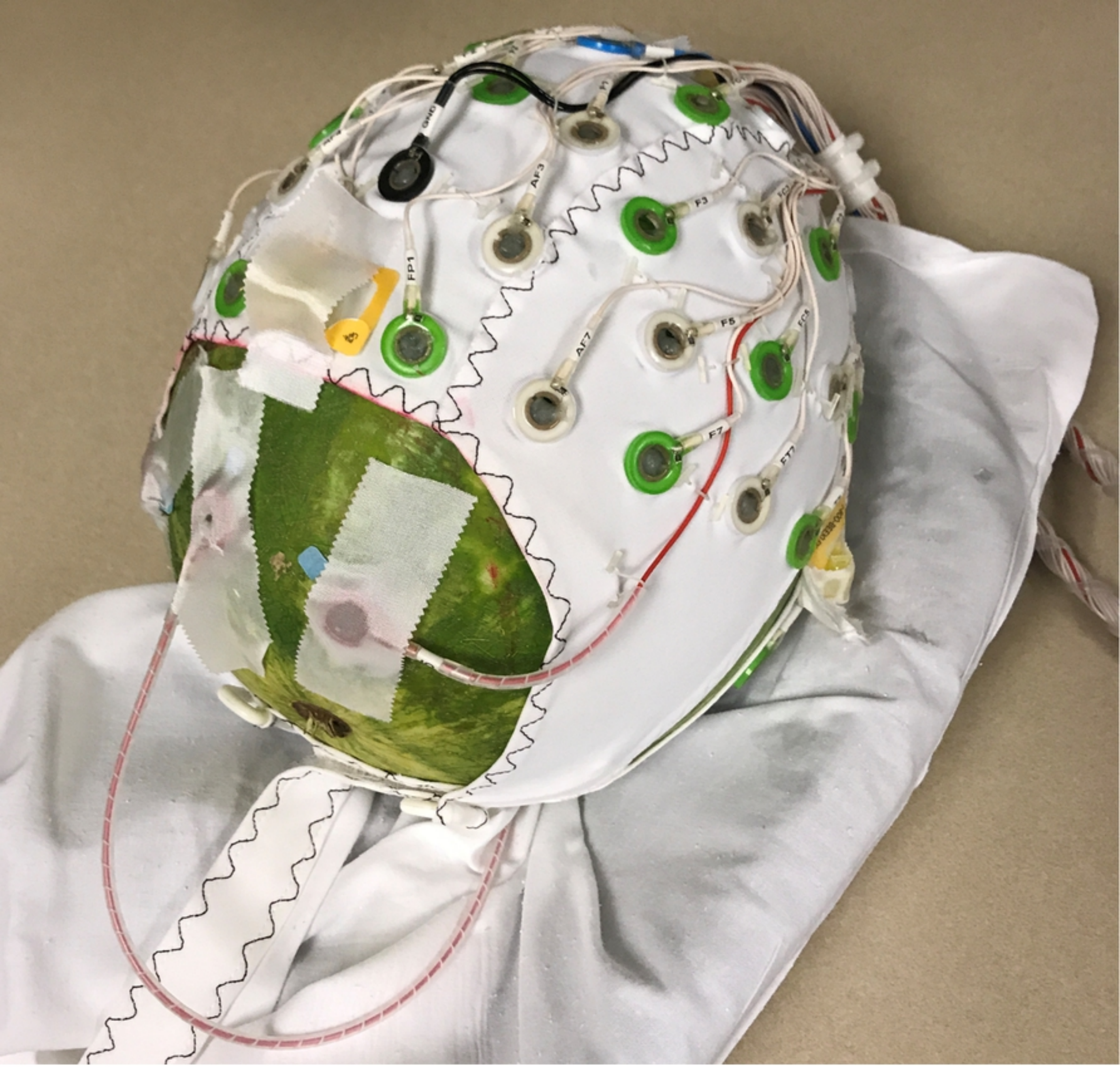

Figure 2

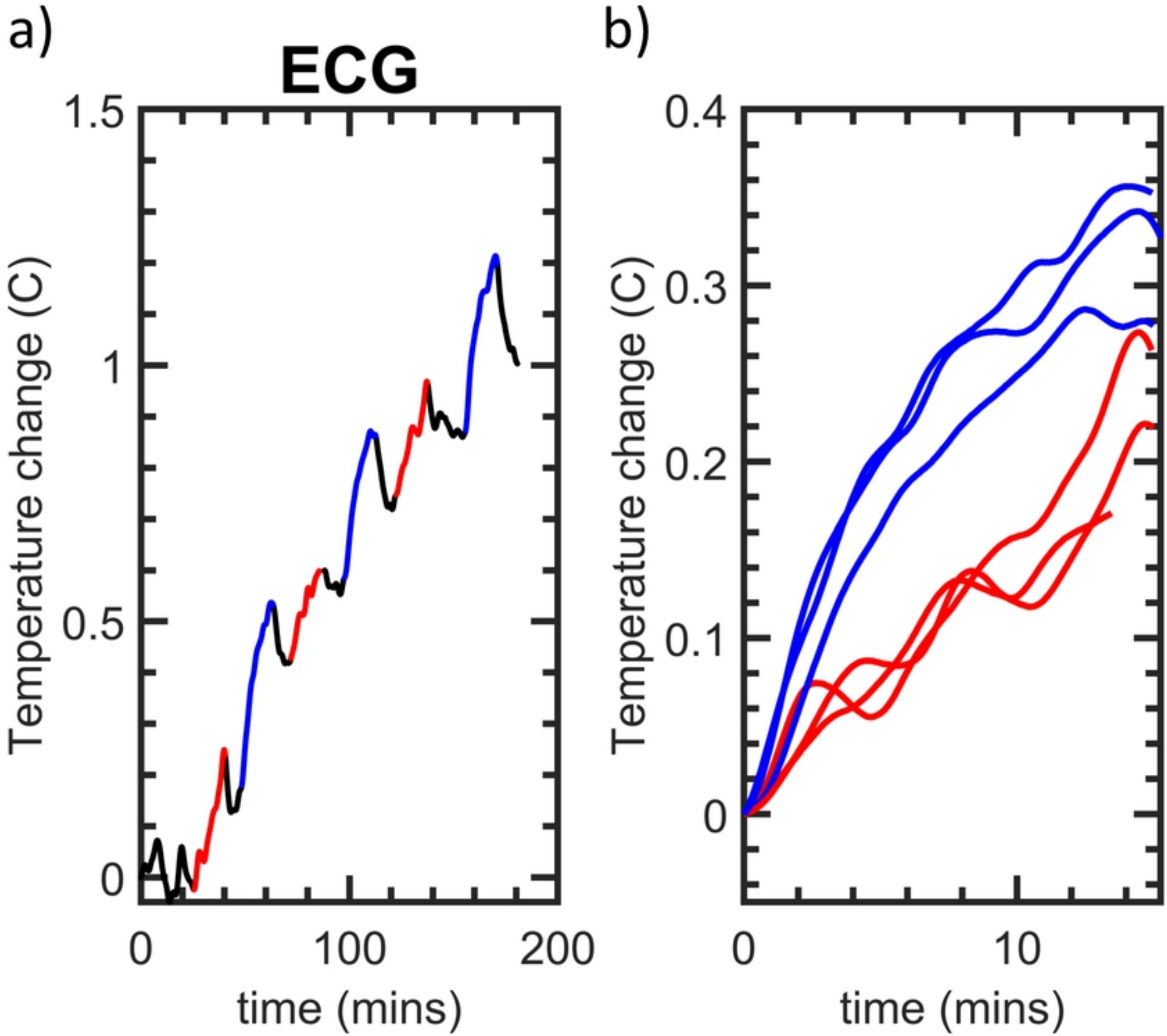
a)
ECG
1.5
1
0.5
0
Temperature change (C)
0
100
200
time (mins)
b)
0.4
0.3
0.2
0.1
0
Temperature change (C)
0
10
time (mins)

Figure 3

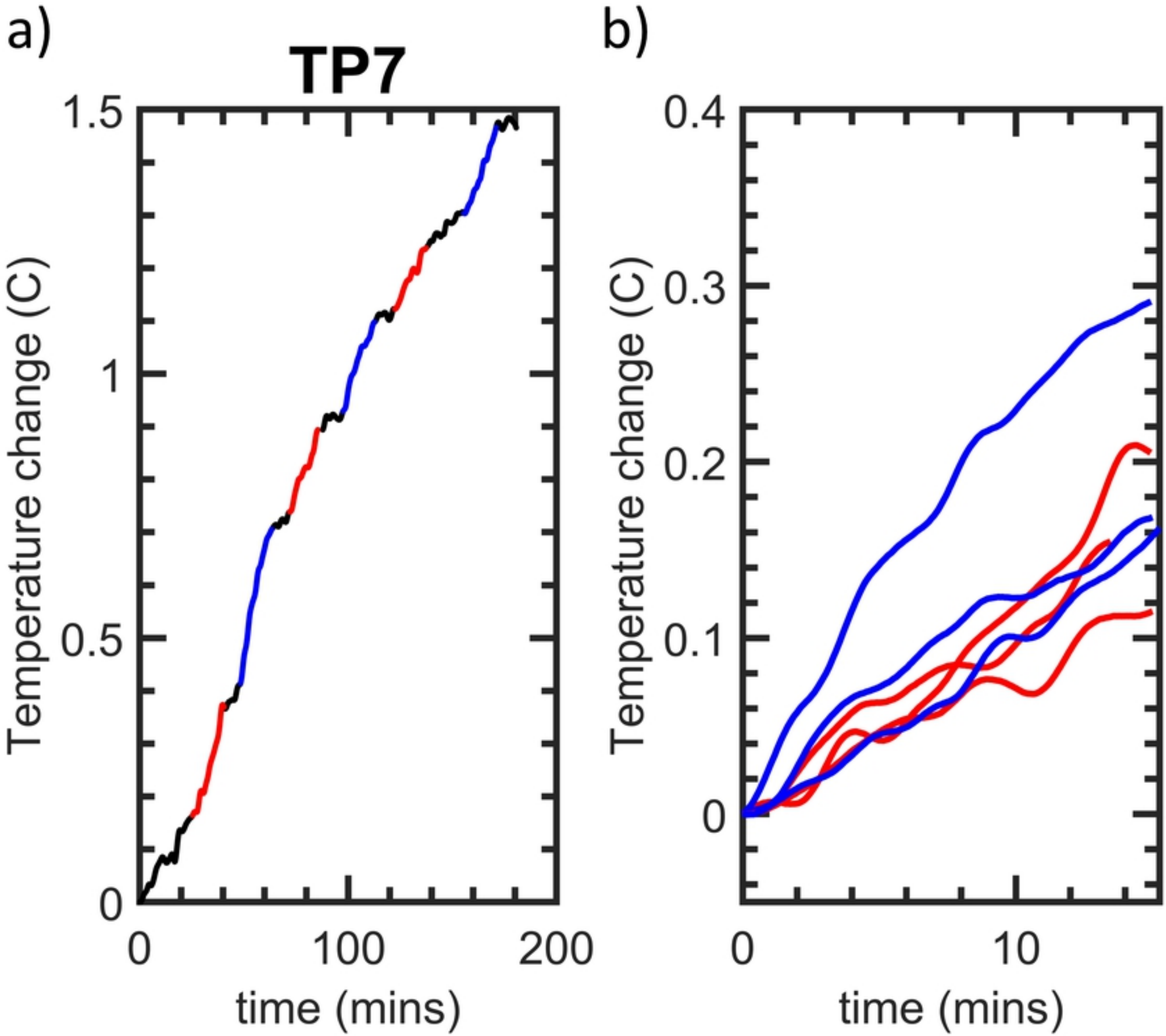
a)
TP7
1.5
1
0.5
0
Temperature change (C)
0
100
200
time (mins)
b)
0.4
0.3
0.2
0.1
0
Temperature change (C)
0
10
time (mins)

Figure 4

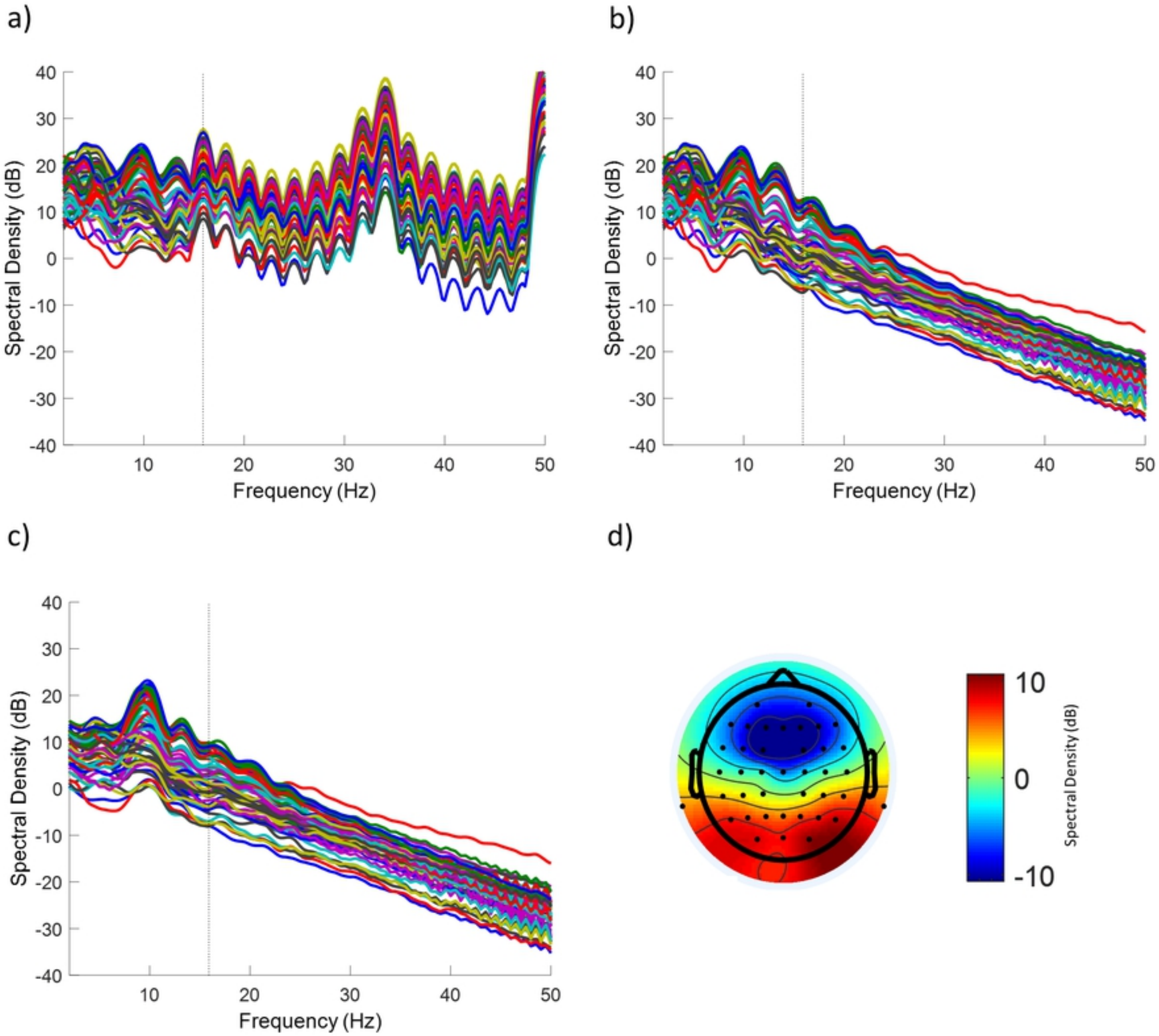
a)
b)
c)
d)
Spectral Density (dB)
Frequency (Hz)
40
30
20
10
0
-10
-20
-30
-40
10
20
30
40
50
Spectral Density (dB)

Figure 5

a)

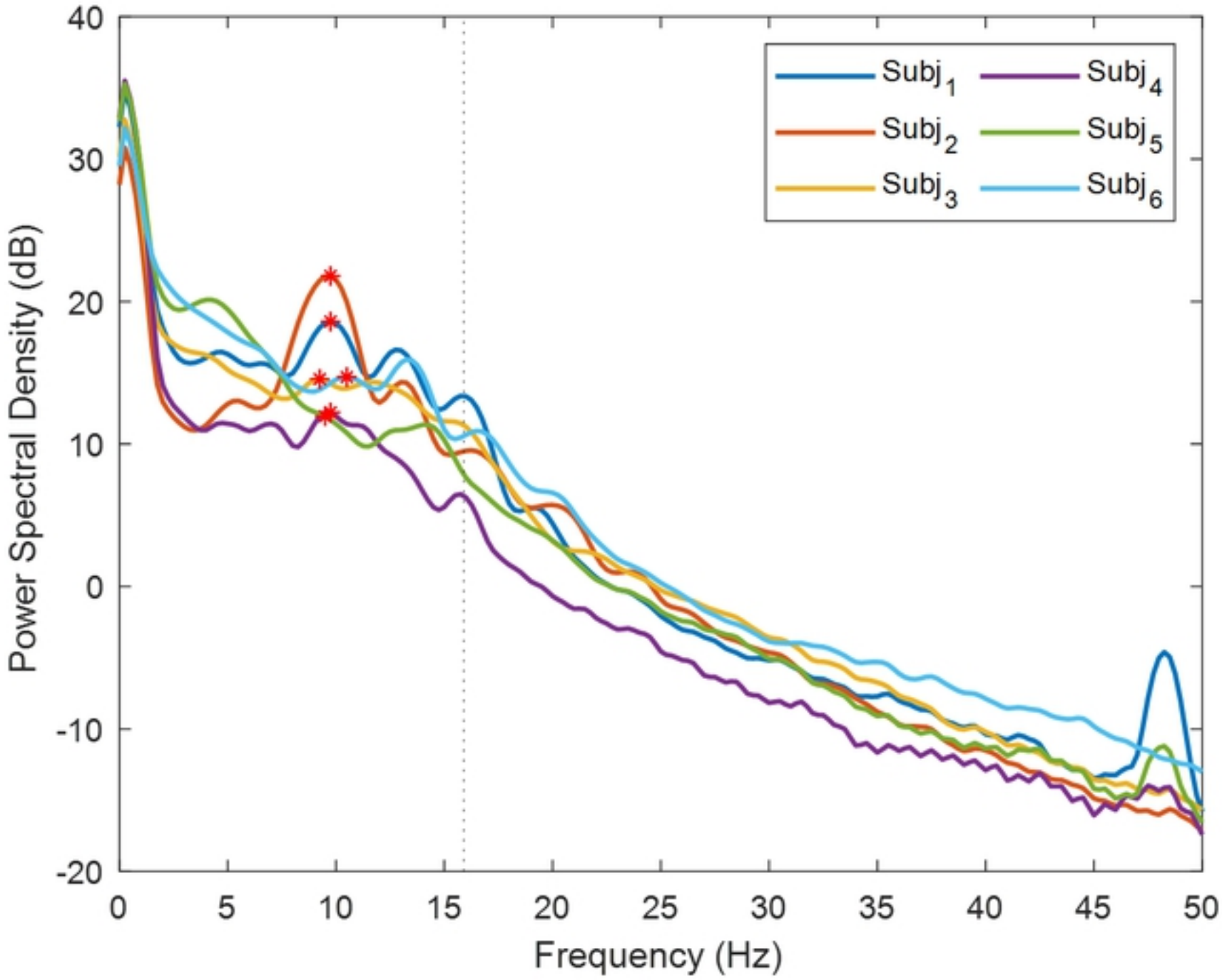
Subj 1
Subj 2
Subj 3
Subj 4
Subj 5
Subj 6
Power Spectral Density (dB)
Frequency (Hz)
40
30
20
10
0
-10
-20
0
5
10
15
20
25
30
35
40
45
50

b)

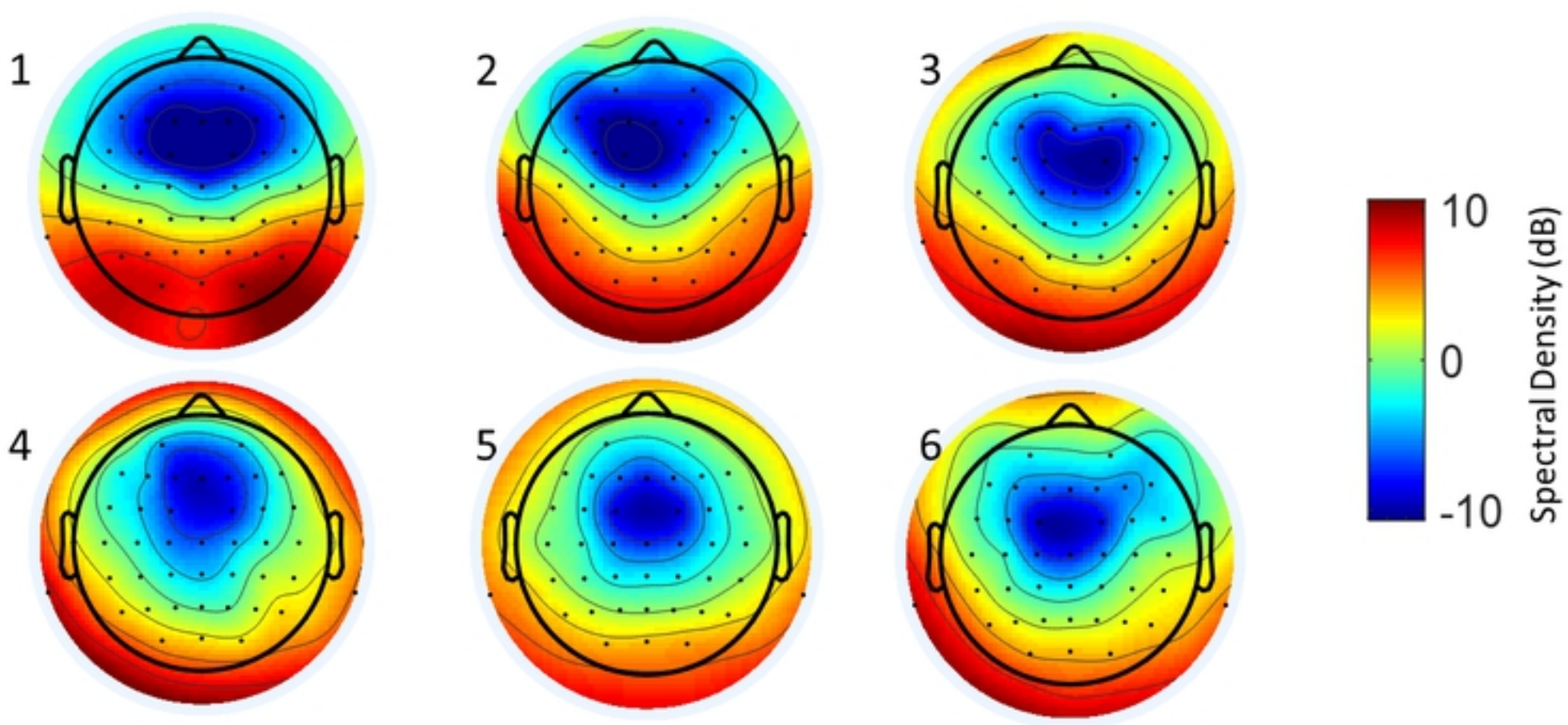
1
2
3
4
5
6
10
0
-10
Spectral Density (dB)

Figure 6